Eur. Phys. J. A **25**, s01, 357–362 (2005)
DOI: 10.1140/epjad/i2005-06-025-1

EPJ A direct
electronic only

Shell structure from ^{100}Sn to ^{78}Ni: Implications for nuclear astrophysics

H. Grawe[1,a], A. Blazhev[1,2], M. Górska[1], I. Mukha[1,3,4], C. Plettner[1,5], E. Roeckl[1], F. Nowacki[6], R. Grzywacz[7], and M. Sawicka[8]

[1] GSI, Planckstr. 1, D-64291 Darmstadt, Germany
[2] University of Sofia, Sofia, Bulgaria
[3] Katholieke Universiteit Leuven, Leuven, Belgium
[4] RRC "Kurchatov Institute", RU-123481 Moscow, Russia
[5] Yale University, New Haven, CT, USA
[6] IReS, Strasbourg, Cedex 2, France
[7] ORNL, Oak Ridge, TN, USA
[8] IEP Warsaw University, Warsaw, Poland

Received: 11 November 2004 / Revised version: 18 February 2005 /
Published online: 25 April 2005 –

Abstract. The single-particle structure and shell gap of ^{100}Sn is inferred from prompt in-beam and delayed γ-ray spectroscopy of seniority and spin-gap isomers. Recent results in ^{94,95}Ag and ^{98}Cd stress the importance of large-scale shell model calculations employing realistic interactions for the isomerism, *np-nh* excitations and $E2$ polarisation of the ^{100}Sn core. The strong monopole interaction of the $\Delta l = 0$ spin-flip partners $\pi g_{9/2}$-$\nu g_{7/2}$ in $N = 51$ isotones below ^{100}Sn is echoed in the $\Delta l = 1$ $\pi f_{5/2}$-$\nu g_{9/2}$ pair of nucleons, which is decisive for the persistence of the $N = 50$ shell gap in ^{78}Ni. This is corroborated by recent experimental data on ^{70,76}Ni, ^{78}Zn. The importance of monopole driven shell evolution for the appearance of new shell closures in neutron-rich nuclei and implications for r-process abundances near the $N = 82$ shell is discussed.

PACS. 21.60.Cs Shell model – 27.30.+t $20 \leq A \leq 38$ – 27.60.+j $90 \leq A \leq 149$ – 26.50.+x Nuclear physics aspects of novae, supernovae, and other explosive environments

1 Introduction

The evolution of shell structure towards exotic nuclei with extreme isospin has become a major topic of experimental and theoretical studies. Especially on the neutron-rich side of the Segré chart, where the drip line is far beyond reach for experiments, the understanding of the underlying shell driving mechanism is of key importance for astrophysics applications as, *e.g.*, the r-process. Two scenarios with differing experimental signature have been proposed to describe the shell structure of nuclei with large N/Z ratios. The first is based on the larger radial extension due to the softer neutron potential. This reduces the spin-orbit (SO) splitting, which is proportional to the potential gradient, for nucleon orbitals probing the nuclear surface [1,2]. It evolves smoothly with A and N/Z and only large variations of these parameters as expected towards the neutron dripline will change the shell structure substantially. The second scenario originates from the strong monopole shifts of selected shell model orbits [3,4,5] and will be discussed in sect. 4. Experimental evidence for monopole driven shell structure is presented in sects. 2 and 3 and generalised to light and r-path nuclei in sect. 4.

2 The ^{100}Sn region

The shell structure of ^{100}Sn and its striking similarity to ^{56}Ni one major shell below has been discussed abundantly [6,7,8]. The study of seniority and spin-gap isomers provides a sensitive probe of single-particle energies, residual interaction, core excitation and shell gaps as demonstrated in recent experiments on ^{98}Cd [9] and ^{94}Ag [10]. The search for a predicted core excited spin trap [11] at the EUROBALL IV array in Strasbourg resulted in the identification of an $I^\pi = (12^+)$ isomer in ^{98}Cd, the two-proton hole neighbour of ^{100}Sn [9]. The inferred level scheme as shown in fig. 1 solves a long-standing puzzle about two largely deviating results for the apparent $I^\pi = (8^+)$ halflife from fusion-evaporation [12] and fragmentation [13] experiments. While the previously non-observed (12^+) isomer masks the measured (8^+) halflife in

[a] Conference presenter; e-mail: h.grawe@gsi.de

Table 1. Observed (EX) and shell model predicted (SM) spin-gap and seniority isomers below ^{100}Sn from $N = Z$ to $N = 50$.

Isotope	E_x (keV)	I^π	Configuration	Decay	Reference
^{94}Pd	4884	14^+	$\pi g_{9/2}^{-4}\nu g_{9/2}^{-2}$	$\gamma(E2)$	EX; [12]
^{95}Pd	1875	$21/2^+$	$\pi g_{9/2}^{-4}\nu g_{9/2}^{-1}$	$\beta\gamma$, $\beta p\gamma$, $\gamma(E4)$	EX; [14,15]
^{96}Pd	2531	8^+	$\pi g_{9/2}^{-4}$	$\gamma(E2)$	EX; [16]
	7040	(15^+)	$\pi g_{9/2}^{-4}\nu g_{9/2}^{-1}d_{5/2}$	$\gamma(E2)$	EX; [16]
^{94}Ag	~ 660	7^+	$\pi g_{9/2}^{-3}\nu g_{9/2}^{-3}$	$\beta\gamma$, $\beta p\gamma$	EX/SM; [10,17,18]
	~ 6600	(21^+)	$\pi g_{9/2}^{-3}\nu g_{9/2}^{-3}$	$\beta\gamma$, $\beta p\gamma$, p, $(2p)$	EX/SM; [10,17,19]
^{95}Ag	2531	$23/2^+$	$\pi g_{9/2}^{-3}\nu g_{9/2}^{-2}$	$\gamma(E3)$	EX; [20]
	4859	$(37/2^+)$	$\pi g_{9/2}^{-3}\nu g_{9/2}^{-2}$	$\gamma(E4)$	EX; [20]
^{96}Cd	~ 5300	16^+	$\pi g_{9/2}^{-2}\nu g_{9/2}^{-2}$	$\beta\gamma$, $\beta p\gamma$	SM; [21]
^{97}Cd	~ 2400	$25/2^+$	$\pi g_{9/2}^{-2}\nu g_{9/2}^{-1}$	$\beta\gamma$, $\beta p\gamma$	SM; [21]
^{98}Cd	2428	8^+	$\pi g_{9/2}^{-2}$	$\gamma(E2)$	EX; [12]
	6635	(12^+)	$\pi g_{9/2}^{-2}\nu g_{9/2}^{-1}d_{5/2}$	$\gamma(E4)$	EX; [9]
^{100}Sn	~ 4200	6^+	$\pi\nu g_{9/2}^{-n}(d_{5/2}, g_{7/2})^n$	$\gamma(E2)$	SM; [9]

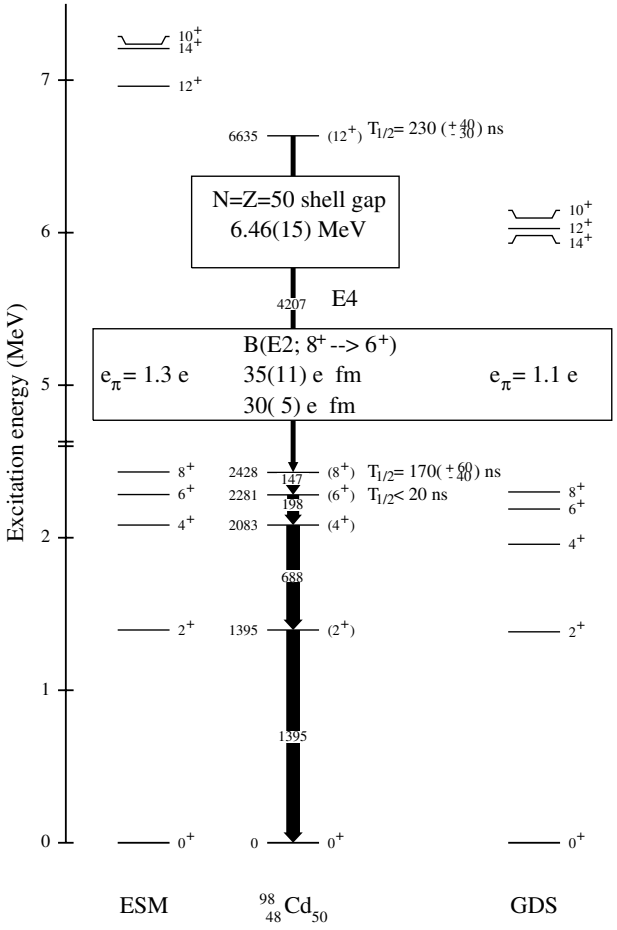

Fig. 1. ^{98}Cd level scheme in comparison to empirical (ESM) and large-scale shell model (GDS) results.

the fusion-evaporation reaction, it is virtually not populated at all in fragmentation of a ^{106}Cd beam [13]. The decay pattern exhibits a striking analogy to ^{54}Fe, two proton holes from ^{56}Ni [6]. The level scheme, the core excited isomer and the $E2$ transition rates are excellently reproduced by a large scale shell model (LSSM) calculation in the $0g$, $1d$, $2s$ model space allowing for up to $4p4h$ excitations of the ^{100}Sn core [9], yielding values of 6.46 (15) MeV for the ^{100}Sn shell gap and a small proton polarisation charge of $\delta e_\pi \leq 0.2e$ (fig. 1).

A second example for the sensitivity of spin-gap isomers to details of the proton-neutron ($\pi\nu$) interaction is provided by the $I^\pi = (21^+)$ state in ^{94}Ag featuring a degree of exotic properties as to spin, excitation energy and decay modes (table 1) [10,17,19], which is unprecedented in the Segré chart. The isomerism is not predicted in the pure $\pi\nu(1p_{1/2}, 0g_{9/2})$ hole space below ^{100}Sn but requires inclusion of core excitations in the *gds* model space. Excellent agreement between LSSM calculations and experiment is observed without any modification of the shell model input. A number of isomers with similar structure have been studied recently between the $N = 50$ and the $N = Z$ lines below ^{100}Sn, such as ^{95}Ag, $I^\pi = (37/2^+)$ [20], ^{96}Ag, $I^\pi = (15^+)$ [22], besides the well-known ^{94}Pd, $I^\pi = 14^+$ [23] and ^{95}Pd, $I^\pi = 21/2^+$ [14,15]. The status of observed isomers and LSSM predicted ones is summarised in table 1. Note the intriguing ^{100}Sn, $I^\pi = 6^+$ $E2$ isomer prediction.

It is the monopole part of the $\pi\nu$ interaction that determines the evolution of the neutron single-particle (hole) energies and the $N = 50$ shell gap upon filling of the $\pi 0g_{9/2}$ orbit from the experimentally known $Z = 40$ region towards $Z = 50$. This provides the key input for the shell model and is further demonstrated in fig. 2. The monopole for a specific multiplet (j, j') is defined by

$$V_{jj'}^m = \sum_J (2J+1)\langle jj'J\,|V|\,jj'J\rangle / \sum_J (2J+1) \qquad (1)$$

which gives rise to the single-particle energy evolution between two shell closures CS and CS' [6]

$$\epsilon_j^{CS} = \epsilon_j^{CS'} + \sum_{j'} (2j'+1-\delta_{jj'})V_{jj'}^m\,. \qquad (2)$$

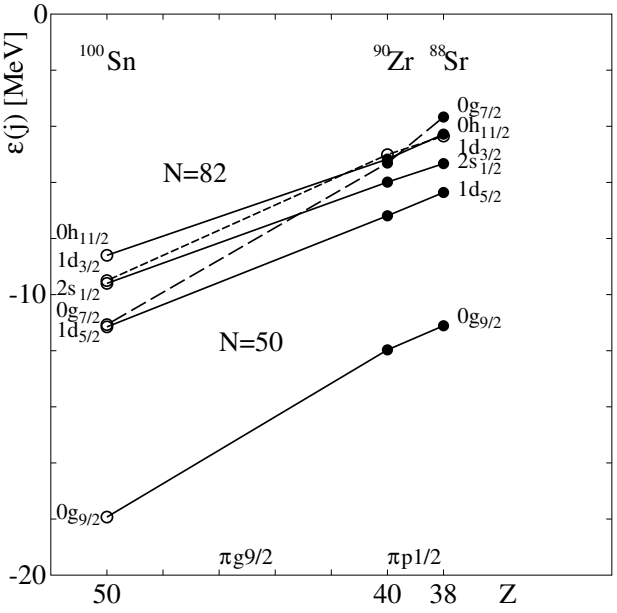

Fig. 2. Evolution of single neutron particle (hole) energies from $Z = 38, 40$ to $Z = 50$. Measured and extrapolated values are indicated by filled and open symbols.

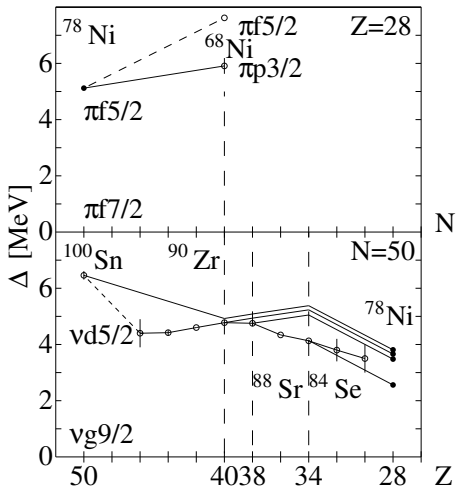

Fig. 3. Evolution of the $Z = 28$ (upper panel) and $N = 50$ (lower panel) shell gaps towards ^{78}Ni. For symbols see fig. 2.

This simple formula can be used to calculate the single-particle energies for ^{100}Sn from the experimentally known ones in ^{90}Zr or ^{88}Sr as shown in fig. 2 for neutrons and a given residual interaction [24]. It should be noted that eq. (2) holds only for closed j' shells, *i.e.* in the example of fig. 2 for the points, in between due to configuration mixing the trend may deviate from the lines drawn to guide the eye. The exact progression can be inferred from a full shell model calculation (see fig. 2 in [11] for the same model space but a modified interaction [25]). In fig. 2 the spin-flip pairs $\pi 0g_{9/2}$-$\nu 0g_{7/2}$, which are spin-orbit partners ($\Delta l = 0$), and $\pi 0g_{9/2}$-$\nu 1d_{3/2}$ ($\Delta l = 2$) exhibit much steeper slopes, *i.e.* comparatively larger monopoles. This is a very general feature of the $\pi\nu$ interaction which is especially strong when the corresponding radial wave functions have good overlap [5,6] (see sects. 3 and 4). We also note that the evolution of neutron single-particle energies from ^{90}Zr ($Z = 40$) to ^{100}Sn ($Z = 50$) and single-hole energies from ^{132}Sn to ^{122}Zr is described by the same interaction only slightly modified due to the different core mass (see sect. 4).

3 Towards ^{78}Ni

On the neutron-rich side of the valley of stability ^{78}Ni, the doubly magic $N = 50$ isotone of ^{100}Sn, has been subject of numerous experimental studies with respect of the persistence of the $N = 50$ shell and its relevance for the astrophysics r-path. Early β-decay results seem to indicate a substantial shell quenching [26], while in-beam experiments on $N \sim 50$ Ge-Se isotopes [27] and isomer studies following fragmentation [28,29,30,31] give evidence for the persistence of the $N = 50$ shell. In β-decay of odd-mass Ni isotopes a strong monopole shift of the $\pi 0f_{5/2}$ level in Cu isotopes upon filling of the $\nu 0g_{9/2}$ shell beyond $N = 40$ was observed [5,6,32]. This is decisive for both the $Z = 28$ and $N = 50$ shell gaps in ^{78}Ni which are determined by the interaction of the spin-flip $\Delta l = 1$ $\pi 0f_{5/2}$-$\nu 0g_{9/2}$ pair of nucleons. In Ni isotopes ($Z = 28$) beyond $N = 40$ by filling of the $\nu 0g_{9/2}$ shell the $\pi 0f_{5/2}$ orbit is bound more strongly than the adjacent $\pi 1p_{3/2}$ and $\pi 0f_{7/2}$ and eventually crosses the $\pi 1p_{3/2}$ to enter the shell gap. Along $N = 50$ the removal of $\pi 0f_{5/2}$ protons will release the $\nu 0g_{9/2}$ stronger than $\nu 1d_{5/2}$ which will reduce the gap. In fig. 3 (lower panel) the extrapolation of the shell gap along the $N = 50$ line from ^{100}Sn to ^{78}Ni for successive removal of the $\pi 0g_{9/2}$, $\pi 1p_{1/2}$, $\pi 1p_{3/2}$ and $\pi 0f_{5/2}$ protons is shown for different experimentally known starting points at $Z = 50, 40, 38, 32$. Monopoles inferred from a realistic $1p$, $0f$, $0g$ interaction [24] were used for $\nu 0g_{9/2}$, whereas the unknown monopoles involving the $\nu 1d_{5/2}$ were taken from a $1d$, $0g$, $1f$ interaction above ^{132}Sn after $A^{-1/3}$ mass scaling. The experimental gaps at $Z = 50, 40, 38$ are well reproduced, and the $N = 50$ gap at $Z = 28$ is extrapolated to be ~ 3.5 MeV, which is reduced by ~ 3.0 MeV from ^{100}Sn (see sect. 2) but still maintains a shell closure. Between the proton subshells the experimental gaps are smaller due to core excitations and configuration mixing as discussed in sect. 2. The shell gap is defined as the energy difference between the highest hole ($\nu 0g_{9/2}$) and the lowest particle ($\nu 1d_{5/2}$) levels. In the upper panel the evolution of the proton gap between $\pi 0f_{7/2}$ and $\pi 0f_{5/2}$ (dashed line), and $\pi 1p_{3/2}$, respectively, is shown, and this latter is the lowest-lying particle orbit at $N = 40$. Therefore, the effect is not as dramatic as along $N = 50$. From $N = 40$ to $N = 50$ the gap is reduced by ~ 1 MeV to ~ 5 MeV, *i.e.* in conclusion the ^{78}Ni shell closure is preserved in agreement with experimental evidence on the persistence of $\nu 0g_{9/2}^2$ seniority isomerism from $N = 42$ (^{70}Ni) to $N = 48$ (^{78}Zn, ^{76}Ni) [28,29,30,31] and the $N = 50$ shell strength in Ge isotopes [27].

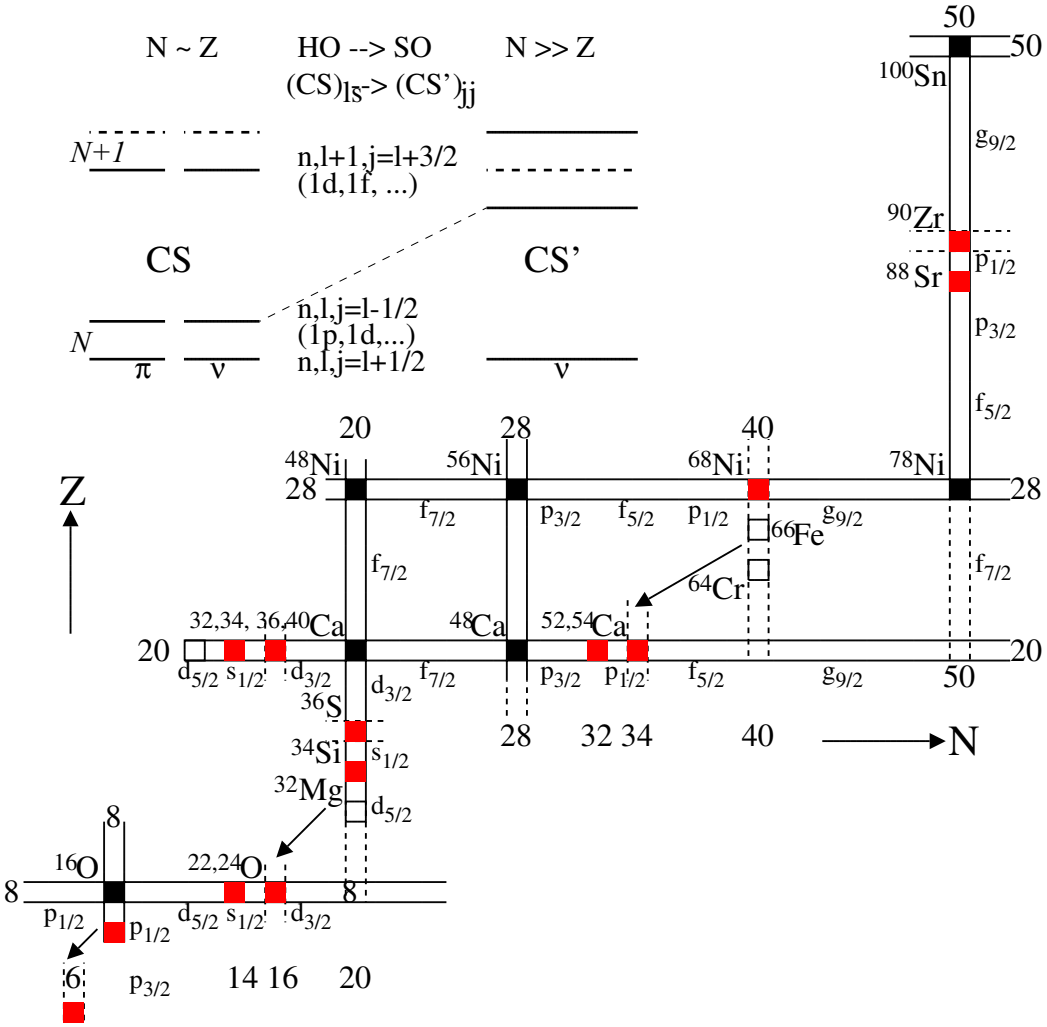

Fig. 4. Schematic chart of known and expected new shell structure in $N \gg Z$ nuclei. The insert illustrates the scenario when moving from $N \sim Z$ closed shells (CS) along isotonic chains to neutron-rich nuclei. Standard (CS) and new closed shell (CS') nuclei are indicated as full and hatched squares. Open squares mark deformed shell quenched nuclei.

The inferred ^{78}Ni shell gaps along with the recently determined empirical $T = 1$ interaction and single-particle (hole) energies for the $N = 50$ isotones and Ni isotopes [33] provide a bench mark for tuning the monopole interaction in the ^{48}Ca to ^{78}Ni model space. The puzzling disappearance of the $I^\pi = 8^+$ isomers in the midshell nuclei ^{72,74}Ni [34], which is intimately connected to the low $I^\pi = 2^+$ excitation energies [6,11], is nicely reproduced by the new $T = 1$ empirical interaction for $Z = 28$ [33].

4 Shell structure towards N ≫ Z

Strong monopole drifts have been experimentally observed all over the Segré chart, the most prominent being the $\Delta l = 0$ spin-orbit $\pi\nu$ pairs $0p_{3/2}$-$0p_{1/2}$, $0d_{5/2}$-$0d_{3/2}$, $0f_{7/2}$-$0f_{5/2}$, $0g_{9/2}$-$0g_{7/2}$ and the $\Delta l = 1$ spin-flip pairs $0p_{1/2}$-$0d_{5/2}$, $0d_{3/2}$-$0f_{7/2}$, $0f_{5/2}$-$0g_{9/2}$, $0g_{7/2}$-$0h_{11/2}$. They are summarised in recent reviews [3,5,6,35] and can be traced back to the $\sigma\tau$ and tensor parts of the NN interaction [3,4]. Recently, based on sound evidence from spectroscopic factors the $\pi 0g_{7/2}$-$\nu 0h_{11/2}$ drift was confirmed, and for the first time a high-spin $\Delta l = 2$ case $\pi 0g_{7/2}$-$\nu 0i_{13/2}$ was established [36]. This translates into the following criteria for strong monopoles: i) the interacting nucleons are spin-flip partners with ii) $\Delta l = 0, 1, 2$ and iii) should have the same number of nodes in their radial wave functions to optimize the overlap. These features are also borne out in realistic interactions as derived from effective NN potentials fitted to scattering data via standard many-body techniques [24] as shown in fig. 17 of [6]. They suffer, however, from the fact that due to the neglect of three-body effects the monopole part is not determined well and has to be tuned to experimental shell evolution, which hampers their predictive power. The dramatic impact of monopole drifts and the sensitivity to subtle details of the interaction is due to the factor $(2j' + 1)$ in eq. (2) which is large in filling (emptying) a high-spin orbital j' and translates

monopole corrections of about 100 keV into MeV. In the following the shell driving by monopole interaction will be discussed for light nuclei (sect. 4.1) and r-path nuclei below ^{132}Sn (sect. 4.2) in a qualitative way.

4.1 New (sub)shells at N = 6, 14/16, 32/34

Based on the above-mentioned criteria the monopole driven shell structure scenario evolves as sketched in the insert of fig. 4. Starting from an $N = Z$ harmonic-oscillator (HO) closed shell nucleus as, *e.g.*, ^{16}O or ^{40}Ca progression along an isotonic chain of semimagic nuclei towards $N \gg Z$ results in:

- Removing protons from a filled ($\pi n, l, j_< = l - 1/2$) orbit, as, *e.g.*, $0p_{1/2}$, $0d_{3/2}$, in a closed shell (CS) will shift the neutron ($\nu n, l + 1, j_> = l + 3/2$) orbit, as, *e.g.*, $0d_{5/2}$, $0f_{7/2}$, upward as its binding is weakened relative to the neighbouring orbits as a consequence of the tensor force. This is due to the $\Delta l = 1$ monopole created by the tensor force [4], which stabilises the shell as, *e.g.*, in ^{14}C, ^{36}S, ^{34}Si and may rearrange the orbitals beyond the closed shell (CS) as observed, *e.g.*, in ^{15}C.
- On further removal of protons from the next lower-lying orbit ($\pi n, l, j_> = l + 1/2$), *e.g.* $0p_{3/2}$, $0d_{5/2}$, its spin-orbit neutron partner $j_<$ ($\Delta l = 0$) will be released in a dramatic way due to the $\sigma\tau$ force to create a new shell CS'.

In summary a HO shell with magic number $N_m = 8, 20, 40$ changes to $N_m - 2 \cdot N = 6, 16(14), 34(32)$ where N is the HO major quantum number. The new magic nuclei are shown as hatched squares in fig. 4. The two-fold closures for $N > 1$ are due to the presence of $j = 1/2$ orbits as $1s_{1/2}$ or $1p_{1/2}$ and the strongly binding $T = 1, j^2$, $J = 0$ two-body matrix-element, which in this case is identical to the monopole. As a consequence according to eq. (2) after filling of the $j = 1/2$ orbit its binding is increased opening another gap. The effect was nicely demonstrated recently for $N = 32, 34$ [4,37]. Experimentally it is well established since long for the pairs of nuclei ^{36}S-^{34}Si ($1s_{1/2}$) and ^{90}Zr-^{88}Sr ($1p_{1/2}$). When further proceeding beyond the point of shell change the previously semi-magic nuclei will develop deformation due to *ph* excitation across the quenched shell gap as indicated by white squares in fig. 4.

Monopole driven shell structure is characterised by the following signature, which substantially deviates from the mechanisms described in the introduction (sect. 1):

- a HO (ls-closed) shell changes to a SO (jj-closed) shell;
- the change is rapid with subshell occupation, and highly localized;
- the scenario is symmetric in isospin projection T_z;
- upon removal of protons the apparent SO splitting between the neutron l, $j_<$ and $j_>$ SO partners ($\Delta l = 0$) due to the $\sigma\tau$ interaction is *increased*, as, *e.g.*, $\nu 0g_{7/2}$-$0g_{9/2}$ upon filling of the $\pi 0g_{9/2}$ shell (see long-dashed lines in figs. 2, 5);
- contrary in the adjacent HO shell $N + 1$ the SO splitting between the l, $j_>$ and $j_<$ is *decreased* due to the tensor force interaction with the $\Delta l = 1$ partner, *e.g.* $\pi 0f_{5/2}$-$0f_{7/2}$ splitting increases when filling the $\nu 0g_{9/2}$ orbit (see dashed line in the upper panel of fig. 3).

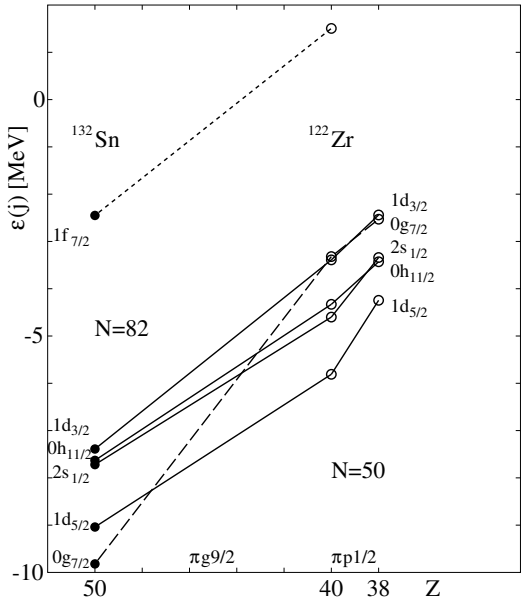

Fig. 5. Evolution of the $N = 82$ shell gap below ^{132}Sn. For symbols see fig. 2.

Further verification is reviewed in refs. [3,5,6,37]. Predictions of this scenario comprise the $N = 32, 34$ closures in Ca isotopes, where first evidence has been presented [38, 39,40], the closure at $N = 14, 16$ in ^{34,36}Ca probing isospin symmetry, and the strongly deformed ^{32}Ca, mirror to ^{32}Mg, ^{66}Fe [41], ^{67}Fe [42] and ^{64}Cr, the $N = 40$ analogues to $N = 20$ ^{32}Mg.

4.2 Implication for structure at the r-path

The success of the concept of monopole driven shell structure especially for the partially quenched $N = 50$ shell at ^{78}Ni, raises the question whether this could provide a possible scenario to understand the r-path abundance deficiency trough below the $A \simeq 130$ peak in astrophysical network calculations [43]. Quenching of the $N = 82$ shell due to a softening of the neutron potential as described in the introduction [2] has been invoked to explain this abundance deficiency [43] and experimental evidence for a reduced shell gap for $N = 82$, $Z \leq 50$ has been presented [44,45]. While the nuclear structure origin of the astrophysics problem is still controversial, it might be appropriate to also look into alternative structure scenarios. In essence a reduced $N = 82$ shell gap causes increased excitation of neutrons into orbitals beyond $N = 82$ leading eventually to deformation. As a consequence the β-decay halflives at the previous waiting points become shorter due to larger Q_β values while they are increased for smaller neutron numbers due to the delayed filling of the $\nu 0g_{7/2}$ subshell which is the key orbital for the $\nu 0g_{7/2} \rightarrow \nu 0g_{9/2}$ allowed Gamow-Teller (GT) transition.

The relevant r-path nuclei are found below ^{132}Sn at $Z \leq 50$ with the single neutron states playing the key role. In fig. 5 the evolution of neutron single-particle (hole) energies around the $N = 82$ shell gap from ^{132}Sn towards ^{122}Zr is shown, where the $\pi 0g_{9/2}$ orbit should be emptied. Starting points are the experimental values adopted for ^{132}Sn [8,6]. The slopes of the neutron hole states are governed by the same $\pi 0g_{9/2}$-νj interaction [24] as for the neutron particles along $N = 50$ as shown in fig. 2 except for a renormalisation due to the different shell model core, which in the simplest case is an $A^{-1/3}$ scaling (see sect. 2). The $\pi 0g_{9/2}$-$\nu 1f_{7/2}$ monopole was scaled up from the $\pi 0h_{11/2}$-$\nu 1g_{9/2}$ interaction at ^{208}Pb [46]. Apparently the shell gap remains unchanged on the way from ^{132}Sn to ^{122}Zr. According to the caveat discussed in connection with eq. (2) and the $N = 50$ shell gap extrapolation in fig. 3 this does not exclude a shell gap reduction due to cross shell excitations when moving away from a doubly magic nucleus along a semi-magic chain of nuclei. Note that from ^{100}Sn to ^{94}Ru this amounts to a ~ 2 MeV reduction (fig. 3) without invoking any additional quenching. The steep upsloping of the $\nu 0g_{7/2}$ level from the deepest in the shell at $Z = 50$ to the Fermi surface at $Z = 40$, however, provides an alternative scenario to explain the same physics as the invoked shell quenching [43]. The allowed GT transition is delayed as the $\nu 0g_{7/2}$ starts to be filled only about 12 nucleons below $N = 82$ thus increasing β-decay halflives in the region $A < 130$. On the other hand a filled $\nu 0g_{7/2}$ orbit at $N \sim 82$ at the Fermi surface causes large effective Q_β values, which decreases the halflives in this region. As a consequence the abundance peak intensities will be shifted to lighter masses.

It should be recalled with respect to the caveat expressed in sect. 2 that this is a qualitative estimate, which hinges on the applicability of eq. (2) and the persistence of a $Z = 40$ subshell in ^{122}Zr. It therefore awaits corroboration by a full shell model calculation employing a monopole tuned realistic interaction, which can be done in less remote nuclei as, *e.g.*, ^{90}Zr, ^{100}Sn and ^{132}Sn in this case.

5 Summary and conclusions

It has been shown that isomer decay spectroscopy close to magic nuclei provides a very sensitive probe of residual interactions and single-particle energies employed in shell model calculations. An indispensable prerequisite for sound predictions are readily available large-scale shell model codes along with realistic interactions that in their monopole part are well adjusted to experimental single-particle energies. This does not hamper the predictive power of shell model calculations as the tuning can be done in regions accessible to detailed spectroscopy (see sects. 3 and 4.2). Monopole driven shell evolution can account for many aspects of structural changes on the pathway from proton-rich $N \sim Z$ nuclei (^{100}Sn) to the neutron-rich $N \gg Z$ (^{78}Ni) region. The concept has been shown to account for the new shell closures established in light nuclei and may provide an alternative access to the structure of r-path nuclei.

References

1. A. Bohr, B.R. Mottelson, *Nuclear Structure* (World Scientific, Singapore, 1998).
2. J. Dobaczewski *et al.*, Phys. Rev. Lett. **72**, 981 (1994).
3. T. Otsuka *et al.*, Phys. Rev. Lett. **87**, 0852502 (2002).
4. T. Otsuka *et al.*, Acta Phys. Pol. B **36**, 1213 (2005).
5. H. Grawe, Acta Phys. Pol. B **34**, 2267 (2003).
6. H. Grawe, Springer Lect. Notes Phys. **651**, 33 (2004).
7. H. Grawe *et al.*, Phys. Scr. T **56**, 71 (1995).
8. H. Grawe, M. Lewitowicz, Nucl. Phys. A **693**, 116 (2001).
9. A. Blazhev *et al.*, Phys. Rev. C **69**, 064304 (2004).
10. C. Plettner *et al.*, Nucl. Phys. A **733**, 20 (2004).
11. H. Grawe *et al.*, Nucl. Phys. A **704**, 211c (2002).
12. M. Górska *et al.*, Phys. Rev. Lett. **79**, 2415 (1997).
13. R. Grzywacz, *Proceedings ENAM98*, AIP Conf. Proc. **455**, 38 (1998).
14. E. Nolte, H. Hicks, Phys. Lett. B **97**, 55 (1980).
15. J. Döring *et al.*, Scientific Report 2003, GSI 2004-1, *Nuclear Structure* (2004) p. 12, and to be published.
16. D. Alber *et al.*, Z. Phys. A **332**, 129 (1989).
17. I. Mukha *et al.*, Phys. Rev. C **70**, 044311 (2004).
18. K. Schmidt *et al.*, Z. Phys. A **350**, 99 (1994).
19. I. Mukha *et al.*, these proceedings.
20. J. Döring *et al.*, Phys. Rev. C **68**, 034306 (2003).
21. K. Ogawa, Phys. Rev. C **28**, 958 (1983).
22. R. Grzywacz *et al.*, Phys. Rev. C **55**, 1126 (1997).
23. M. Górska *et al.*, Z. Phys. A **353**, 233 (1995).
24. M. Hjorth-Jensen *et al.*, Phys. Rep. **261**, 125 (1995) and private communication.
25. M. Górska *et al.*, *Proceedings ENPE99*, AIP Conf. Proc. **495**, 217 (1999).
26. K.-L. Kratz *et al.*, Phys. Rev. C **38**, 278 (1988).
27. Y.H. Zhang *et al.*, Phys. Rev. C **70**, 024301 (2004).
28. R. Grzywacz *et al.*, Phys. Rev. Lett. **81**, 766 (1998).
29. J.M. Daugas *et al.*, Phys. Lett. B **476**, 213 (2000).
30. M. Sawicka *et al.*, Eur. Phys. J. A **20**, 109 (2004).
31. R. Grzywacz, these proceedings.
32. S. Franchoo *et al.*, Phys. Rev. C **64**, 054308 (2001).
33. A. Lisetskiy *et al.*, Phys. Rev. C **70**, 044314 (2004); these proceedings.
34. M. Sawicka *et al.*, Phys. Rev. C **68**, 044304 (2003).
35. T. Otsuka *et al.*, Eur. Phys. J. A **15**, 151 (2002).
36. J.P. Schiffer *et al.*, Phys. Rev. Lett. **92**, 162501 (2004).
37. M. Honma *et al.*, Phys. Rev. C **69**, 034335 (2004); these proceedings.
38. R.V.F. Janssens *et al.*, Phys. Lett. B **546**, 55 (2002).
39. S.N. Liddick *et al.*, Phys. Rev. Lett. **92**, 072502 (2004).
40. P. Mantica, these proceedings.
41. M. Hanawald *et al.*, Phys. Rev. Lett. **82**, 1391 (1999).
42. M. Sawicka *et al.*, Eur. Phys. J. A **16**, 151 (2002).
43. B. Pfeiffer *et al.*, Nucl. Phys. A **693**, 282 (2001).
44. I. Dillmann *et al.*, Phys. Rev. Lett. **91**, 162503 (2003).
45. T. Kautzsch *et al.*, Eur. Phys. J. A **9**, 201 (2000).
46. E.K. Warburton *et al.*, Phys. Rev. C **44**, 233 (1991).